NANO · MICRO small
www.small-journal.com

Study of DNA Origami Dimerization and Dimer Dissociation Dynamics and of the Factors that Limit Dimerization

*Miran Liber, Toma E. Tomov, Roman Tsukanov, Yaron Berger, Mary Popov, Dinesh C. Khara, and Eyal Nir**

Organizing DNA origami building blocks into higher order structures is essential for fabrication of large structurally and functionally diverse devices and molecular machines. Unfortunately, the yields of origami building block attachment reactions are typically not sufficient to allow programed assembly of DNA devices made from more than a few origami building blocks. To investigate possible reasons for these low yields, a detailed single-molecule fluorescence study of the dynamics of rectangular origami dimerization and origami dimer dissociation reactions is conducted. Reactions kinetics and yields are investigated at different origami and ion concentrations, for different ion types, for different lengths of bridging strands, and for the "sticky end" and "weaving welding" attachment techniques. Dimerization yields are never higher than 86%, which is typical for such systems. Analysis of the dynamic data shows that the low yield cannot be explained by thermodynamic instability or structural imperfections of the origami constructs. Atomic force microscopy and gel electrophoresis evidence reveal self-dimerization of the origami monomers, likely via blunt-end interactions made possible by the presence of bridging strands. It is suggested that this mechanism is the major factor that inhibits correct dimerization and means to overcome it are discussed.

1. Introduction

The DNA origami technique has been demonstrated to be very useful for rational and programmable organization of matter with atomic and molecular precision in ways that were unimaginable until recently.[1–4] DNA origami frameworks enable organization of proteins,[5–7] carbon nanotubes,[8,9] metallic nanostructures,[10–14] and other molecules.[15] DNA-based molecular machines, motors, and other devices that can perform complex operations and tasks have been constructed using DNA origami;[16–18] these include a molecular assembly line,[19] a nanorobot for targeted drug delivery,[20] a DNA nanochip for base-excision repair,[21] molecular sorting robots,[22] and devices that measure intermolecular and intramolecular forces,[23,24] to name a few. These constructs and devices were made from single origami units, a fabrication approach that limits the size of the construct and its chemical addressability in comparison to a Lego-like assembly of different and diverse origami units.

To overcome size limitations, identical origami building blocks have been polymerized into linear or 2D structures, achieving structures with hundreds of building blocks.[25–29] However, with this approach, the origami building blocks are free to polymerize uncontrollably. To enable addressability and control of size, origami building blocks with unique connectivities have been prepared separately and then mixed to form defined structures.[1,29–41] Typically programed connectivity is achieved by hybridization of DNA strands with unique nucleotide (nt) sequences, called bridging strands, but desired connectivity can also be achieved by using complementary origami shapes and blunt-end stacking interactions.[34–36,39–41] In principle, this approach should allow Lego-like assembly of structures with almost any desired architecture and size. In practice, however, the assembly yields of structures prepared using the strand hybridization method are typically low (e.g., 80–90% for dimers,[30,37,42] 50% for trimers,[34,35] and 35% for construct with nine building blocks[34]), significantly restricting the size of the assembled construct to a small number of units. In one study, a dimerization yield of 96% was achieved using an elevated Mg^{2+} concentration (60×10^{-3} M).[43] However, this high Mg^{2+} concentration may result in nonspecific origami aggregation and cannot always be employed.

In a recent study, Tikhomirov et al. constructed an 8 × 8 origami array made of 64 unique origami tiles using blunt-end stacking interactions approach.[40] The dimerization yield was 95%, and the total yield was 4%. Interestingly, the blunt-end interactions in these systems were significantly weaker than

Dr. M. Liber, Dr. T. E. Tomov, Dr. R. Tsukanov, Dr. Y. Berger, Dr. M. Popov, Dr. D. C. Khara, Prof. E. Nir
Department of Chemistry and the Ilse Katz Institute for Nanoscale Science and Technology
Ben-Gurion University of the Negev
Beer Sheva 84105, Israel
E-mail: eyalnir@bgu.ac.il
The ORCID identification number(s) for the author(s) of this article can be found under https://doi.org/10.1002/smll.201800218.

DOI: 10.1002/smll.201800218

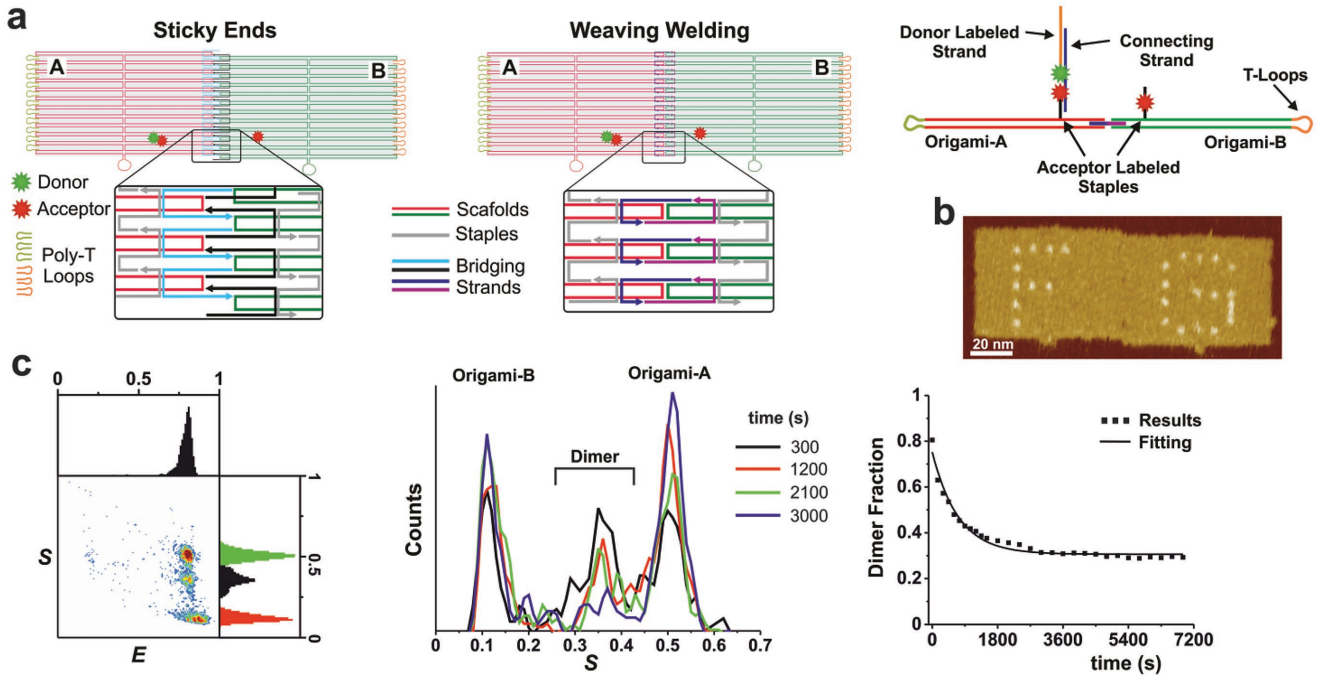

Figure 1. Origami dimerization techniques and single-molecule measurement. a) Schematics of dimers made by sticky end and weaving welding techniques and a dimer side view. The positions of the donor and acceptor fluorophores are shown as green and red stars, respectively. Bridging strands for SE and WW are shown in cyan, black, dark blue, and purple. Poly-T loop staples were incorporated at the edges opposite the dimerization edge to prevent nonspecific origami binding. b) Illustrative AFM image of origami-A/origami-B dimer formed using the SE technique. These monomers were without the labeled strands but with "F" and "G" marking. c) Typical 2D *E*/*S* histogram and *E* and *S* projections (left panel). Origami-A, origami-B, and the dimer populations are shown in the *S* projection (green, red, and black histograms, respectively). Typical *S* projection histograms measured at different times after initiation of the dissociation reaction (middle panel). Kinetic profile of the dimer dissociation reaction calculated from the size of the monomer and dimer populations (right panel). Dimerization reactions were fitted using second-order reaction model, and dimer dissociation reactions were fitted using a first-order reaction model (black curve, right panel) throughout this work (Equations (1) and (2), respectively).

strand hybridization typically used for origami attachment. The authors of this work suggest that the weak stacking interactions allowed rearrangements that helped building blocks escape kinetic traps during array assembly.

We have developed a bipedal motor that can walk back and forth over 370 nm on a track made of a single origami unit,[44] and our recent (unpublished) motor design allows even longer walking distances. To enable unidirectional walking for such long distances, the track has to be made from several unique origami tiles. Unfortunately, we are able to achieve only about 86% yield for origami dimers (and about 64% for trimmers), making many of the tracks shorter than the distance our walkers can cross. This emphasizes the need for improved origami building-block assembly methods. The dynamics of the origami attachment reaction have been studied,[30,31,45] but the reason for the low yields remains unknown.

Here we studied the mechanisms that may prevent the formation of origami dimers at high yields. We designed two different rectangular origami monomers that can be attached to each other via strand hybridization (23 or 24 bridging strands with interacting segments of the lengths 5, 8, or 11 nts). Dimerization was initiated by mixing of the two monomers at conditions in which there was no dimer dissociation. Under these conditions, the dimerization yields were only about 79–86% and were independent on the lengths of the interacting segments, indicating that thermodynamic instability is not the reason for the low yield. Atomic force microscopy (AFM) data showed that a small fraction of the monomers are structurally imperfect; however, the independence of dimerization yields on the number of hybridizing nucleotides in our systems indicates that these structural imperfections cannot explain the observed low dimerization yields. Rather, we provide gel electrophoresis and AFM evidence for nonspecific self-dimerization of monomers and suggest that this is likely the major reason for the low yield of the correct dimers.

2. Results and Discussion

2.1. Origami Monomer Design

The origami monomers were based on the Rothemund rectangle origami[1] with minor modifications and were assembled by temperature-gradient annealing followed by size-exclusion chromatography purification (for details, see the Supporting Information). Origami-A and origami-B monomers were each prepared with 12 unique bridging strands incorporated into one of the origami edges and 12 strands containing poly-T loops (6-12 Ts) incorporated into the opposite side (**Figure 1**a). The T loops reduce nonspecific origami dimerization that may be caused by blunt-ends stacking of the origami edges.[1,37,46] Staples, bridging strands, and T-loop strands (purchased from

IDT) were used unpurified, and the scaffold was M13mp18 (New England BioLabs).

2.2. Origami Attachment Techniques

Schematics of the "sticky end" (SE)[25,30,31,33] and the "weaving welding" (WW)[1,26–29,34–37,43] origami attachment techniques are presented in Figure 1a. In the sticky ends technique, each of the bridging strands was hybridized in its middle to the origami scaffold via 32 base pairs during the annealing process, leaving two overhanging sticky ends. The lengths of the sticky ends used in this work were 5, 8, and 11 nts (SE-5, SE-8, and SE-11, respectively). With this design, origami dimers were formed via hybridization of the 23 sticky ends of origami-A with the complementary 23 sticky ends of origami-B forming a total of 23 connections (Figure 1a,b). In the weaving welding technique, each of the bridging strands was hybridized to the origami scaffold via 24 base pairs, leaving a single overhang with a length that matched the length of the complementary scaffold segments of the other origami (in this work, 8 nucleotides, called WW-8). With this design, dimers form by weaving and welding of the overhangs of the bridging strands attached to one origami with the scaffold of the other,[26,37] forming a total of 24 connections. The base compositions of the WW overhangs were about 50% guanine and cytosine bases (GC) and those of the SE overhangs were generated randomly but such that the GC content for each sequence was about 50%. NUPACK[47] analysis of the sticky end sequences showed that none of the sequences self-hybridized or cross-hybridized at more than 0.1%.

2.3. Single-Molecule Fluorescence Measurements

The kinetics and yields of origami dimerization and dissociation reactions were studied using the diffusion-based single-molecule alternating laser excitation (ALEX) technique coupled with Förster resonance energy transfer (FRET) technique. With this method, a donor excitation laser excites the donor fluorophore (ATTO-550, ATTO-TECH) alternately with an acceptor excitation laser that excites the acceptor fluorophore (ATTO-647N). The ratio of photons detected during the two time periods reports on the donor/(donor + acceptor) stoichiometry ratio (S). For detailed descriptions of the instrumentation, method, and definition of S and FRET value (E), see Equations S1 and S2 of the Supporting Information, and our previous publications.[18,37,48,49]

Origami-A and origami-B were labeled with acceptor fluorophore by introduction of acceptor-labeled elongated staples during annealing (Figure 1a; Tables S1 and S2, Supporting Information). In addition, origami-A was labeled with donor fluorophore-conjugated strand by hybridization to the acceptor-labeled strand via a connecting strand. With this design, origami-A, origami-B, and the dimer species yielded signals (photon bursts) with different fluorophore stoichiometry ratios (centered on $S = 0.5$, 0.1, and 0.35, respectively, Figure 1c, left and middle panels), allowing determining the relative ratio of monomer and dimer populations in the solution. The usage of ALEX/FRET rather than only FRET allowed us to place the fluorophores deeper inside the origami structure, and the stoichiometry signal reports on the presence or absence of the origami monomers main body and not labeled bridging strands as would be the case using only FRET. The high FRET values of origami-A ($E \approx 0.8$, Figure 1c, left panel) improve the resolution of the ALEX method as previously described.[49]

2.4. Measurement of Reaction Kinetic Profiles

Reaction kinetics were monitored by measuring the relative population sizes of the origami-A, origami-B, and dimer species at different times after the initiation of the dimerization or dissociation reaction (Figure 1c, middle and right panels). The kinetic profiles were calculated by dividing the size of the dimer population (S_{Dimer}) by the sum of the dimer and the acceptor-labeled monomer (origami-B; $S_{\text{Dimer}} + S_{\text{Origami - B}}$) at different reaction times.

2.5. Origami Dimerization Kinetics and Yield

Origami dimerization reactions were initiated by mixing equimolar concentrations of origami-A and origami-B (typically 0.75×10^{-9} M) at a certain NaCl concentration (typically 250×10^{-3} M) and at room temperature. Small fractions of the mixture were sampled at different reaction times and diluted to 15×10^{-12} M origami and a certain NaCl concentration (typically 40×10^{-3} M NaCl), and monomer and dimer constructs were monitored using the single-molecule technique (20–40 min for each measurement). Unless mentioned otherwise, these were the default conditions. The kinetic profiles were fitted using a second-order reaction model with a second-order dimerization rate constant (k_{dim}) and a maximum reaction yield (defined as the fraction of dimers at infinite time, DF_{inf}) as free fitting parameters (see the Experimental Section and Equation (1)). There was no dimer dissociation in the dimerization or measurement conditions (as we show below), and, therefore, the fitting did not include dissociation reaction component.

We studied dimerization of the rectangular origami using the sticky end method at different NaCl concentrations (**Figure 2**a), with different lengths of sticky ends (Figure 2b), at different origami monomer concentrations (Figure 2c) and at 10×10^{-3} M Mg^{2+} concentration (Figure 2d). In addition, we studied dimerization using the weaving welding technique under the default conditions (Figure 2b). The results (for SE-8) showed that increasing the NaCl concentration (from 50 to 2000×10^{-3} M, which is above the dissociation threshold, see below) increased the dimerization rate by approximately an order of magnitude (from $k_{\text{dim}} = 0.5 \times 10^6$ M^{-1} s^{-1} to $k_{\text{dim}} = 8.0 \times 10^6$ M^{-1} s^{-1}, Figure 2e). The dimerization rate increased with origami monomer concentration (although not linearly, Figure 2c). Importantly, above 50×10^{-3} M NaCl, increased NaCl concentration increased the dimerization yield by only a few percent (for SE-8, $DF_{\text{inf}} = \approx 0.76 - 0.83$, Figure 2e), and the yield essentially plateaued above 500×10^{-3} M NaCl. Dimerization in the presence of 10×10^{-3} M Mg^{2+} yielded rates similar to that of dimerization in 70–80 $\times 10^{-3}$ M NaCl ($k_{\text{dim}} = 1.87 \times 10^6$ $M^{-1}s^{-1}$). Importantly, our results show that increased length of the sticky ends (from

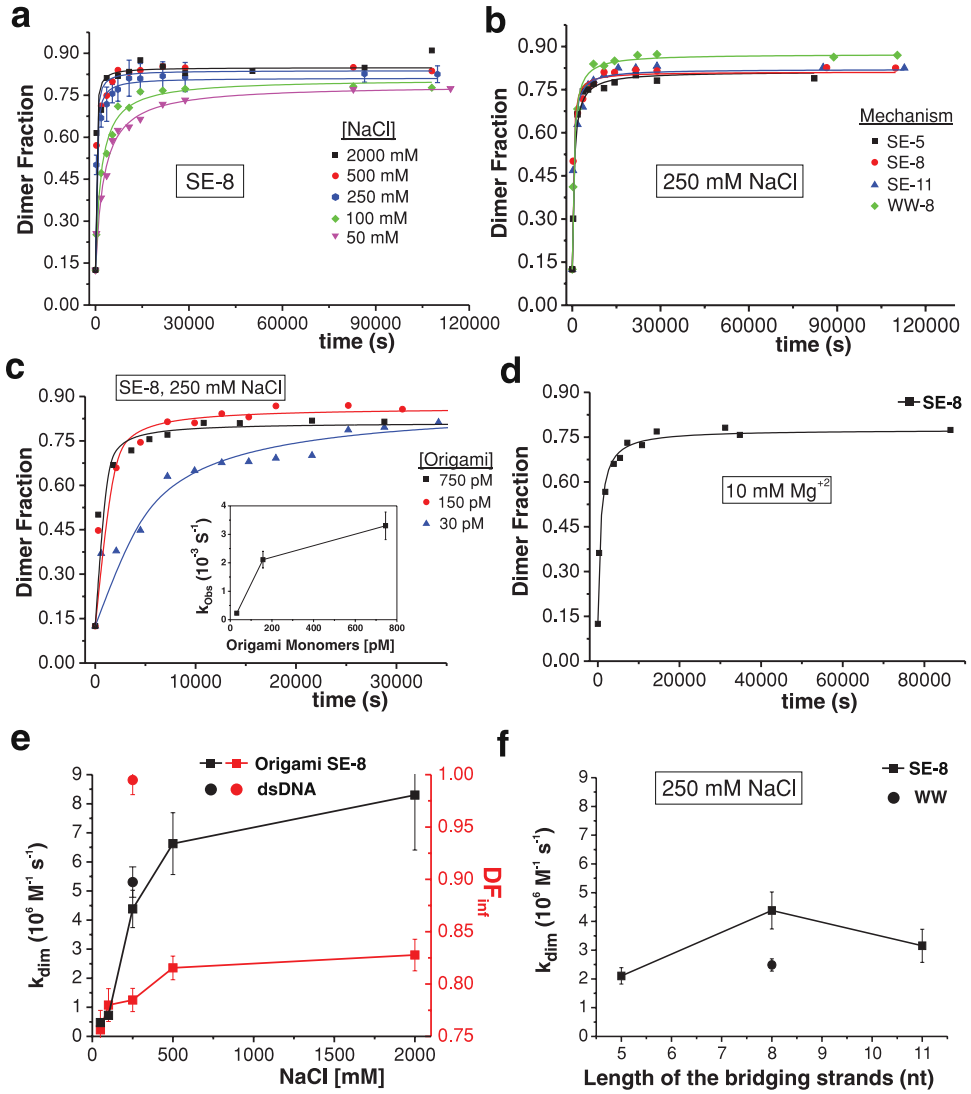

Figure 2. Dynamics of origami dimerization. a) Kinetic profiles of origami sticky end (SE-8) dimerization reactions at different NaCl concentrations. b) Kinetic profiles of SE-5, SE-8, SE-11, and WW-8 dimerization reactions at 250×10^{-3} M NaCl. c) Kinetic profiles of dimerization reactions of different concentrations of SE-8 at 250×10^{-3} M NaCl. The observed rates (k_{Obs}) are summarized in the inset. d) Kinetic profiles of dimerization reactions of SE-8 at 10×10^{-3} M Mg^{2+} concentration. e) Summary of the dimerization rate constants (k_{dim}, black) and of the reaction yield (DF_{inf}, red). Also shown are the rates and yields of complementary DNA strand hybridization (dsDNA, circles, see Figure S1 of the Supporting Information). f) Rates (k_{dim}) for origami dimerization as a function of length of bridging strands for SE and WW attachment techniques. The origami monomer concentrations in experiments shown in panels (a), (b), and (d) were 0.75×10^{-9} M. Measurements shown in panels (a) and (b) were conducted at 40×10^{-3} M NaCl, except for SE-5 (250×10^{-3} M). The lines in panels (a)–(d) are the best fits of the results with a second-order reaction model (Equation (1)). Standard deviations are shown for selected data. The signal at time zero was due to background signal rather than dimer (see Figure S3 of the Supporting Information).

5 to 11 nts) did not increase the yields of the dimerization reaction (Figure 2b, in dimer-favorable conditions). The dimerization yield for the weaving welding method was slightly higher than that of the sticky end method (DF_{inf} = 86%, and DF_{inf} = 79%, respectively, Figure 2b), but dimerization rates were within the range of that of the sticky ends (Figure 2f) at the same NaCl concentration (250×10^{-3} M). For comparison, we measured the hybridization of two DNA strands (designed to form a 40-base-pair duplex) at the default conditions using the ALEX method (Figure S1, Supporting Information). The yield for DNA strand hybridization was around 99% (Figure 2e; Figure S1, Supporting Information), which is close to the 100% expected from the free energy of hybridization of these strands (calculated using MFOLD[50]). The measured hybridization rate was in agreement with published rates.[51,52] These results validate our ALEX method and demonstrate that the low origami dimerization yields observed are not a result of experimental artifacts (e.g., bleached fluorophores, limitations of the ALEX method).

2.6. Origami Dimer Dissociation Kinetics and Yield

To further understand the stability of origami dimers and to characterize the dissociation conditions (necessary for the

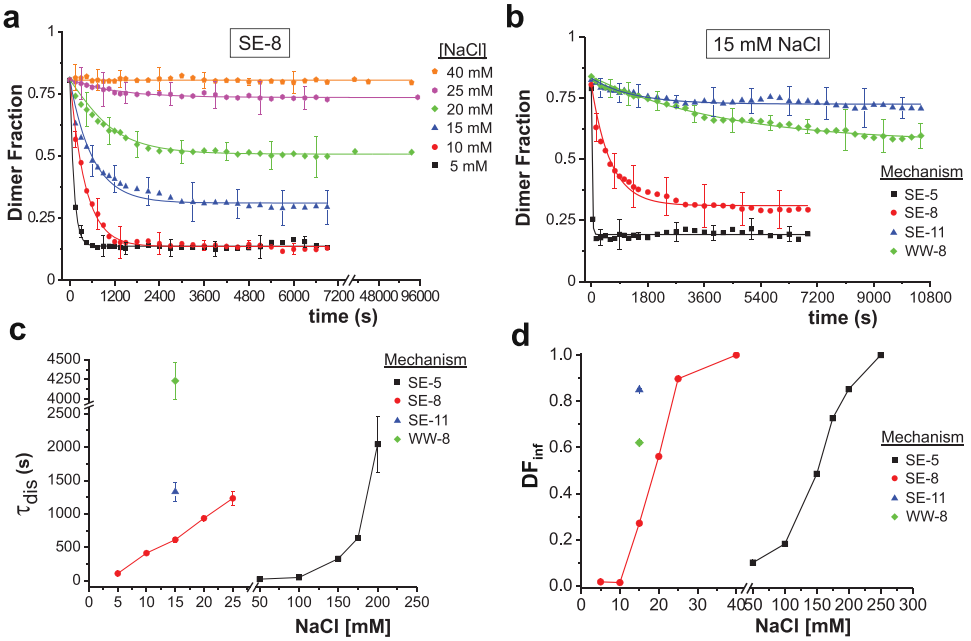

Figure 3. Dynamics of origami dimer dissociation. a) Kinetic profiles of sticky end dimer (SE-8) dissociation reactions at different NaCl concentrations. b) Kinetic profiles of SE-5, SE-8, SE-11, and WW-8 dimer dissociation reactions measured at 15×10^{-3} M NaCl. The dimer concentrations were 15×10^{-12} M. The lines are the best fits of the data with first-order dissociation reaction model (Equation (2)). The residual profiles did not reach zero values because of background signal; see Figure S3 of the Supporting Information. c,d) Dissociation time constants (τ_{dis}) and yields at infinite time (DF_{inf}) determined by the fitting. For the kinetic profiles of SE-5, see Figure S5 of the Supporting Information. Standard deviations are shown for selected data. Some of the error bars are smaller than the symbols in panels (c) and (d).

design of the dimerization experiments and analysis of the dynamics), we performed single-molecule fluorescence dissociation kinetic experiments. First, dimers were prepared by mixing 0.75×10^{-9} M origami-A and origami-B in 250×10^{-3} M NaCl for at least 24 h, allowing completion of the dimerization reaction (as shown in Figure 2). A small fraction of the dimer solution was then diluted to 15×10^{-12} M dimer concentration in measurement buffer that contained a certain concentration of NaCl and that was prepositioned on the optical setup. The sample was then monitored continuously, and data points were calculated for selected time segments within the measurement. The dissociation conditions were selected such that there was no dimerization (for example, see Figure S4 of the Supporting Information for SE-8). Therefore, the kinetic profiles were fitted using first-order dissociation reaction models with time constant (τ_{dis}) and dimer yield at infinite time (DF_{inf}) as free fitting parameters (see the Experimental Section and Equation (2)).

In NaCl concentrations equal to (or higher than) 40×10^{-3} M, the SE-8 dimers did not dissociate (**Figure 3**a). At NaCl concentrations lower than 40×10^{-3} M, the SE-8 dissociation rate increased as NaCl concentration decreased (Figure 3c). Interestingly, although there was no dimerization at or below 40×10^{-3} M NaCl (Figure S4, Supporting Information), not all dimers dissociate. The fraction of dimers plateaued to a certain level, with DF_{inf} values decreasing with increased NaCl concentration (Figure 3a,d). Shorter sticky ends resulted in significantly faster dissociation and lower fractions of dimer (e.g., for 15×10^{-3} M NaCl, Figure 3b–d). At 40×10^{-3} M NaCl, for example, SE-8 did not dissociate whereas at 50×10^{-3} M NaCl, conditions in which the dimers are more stable, SE-5 dissociated almost completely (Figure 3d). Comparison of the weaving welding and the sticky ends techniques showed that for the same number of base pairs formed (as in WW-8 and SE-8) the sticky ends dimers dissociated more rapidly and to lower dimer fractions than the weaving and welding dimers (Figure 3b–d).

2.7. Low Dimerization Yield Is not a Result Thermodynamic Instability

Two lines of evidence support our conclusion that the low yield observed for dimerization is not a result of equilibrium between dimer association and dissociation reactions. First, in conditions that are significantly more dimer-favorable than the threshold conditions for dissociation, the dimerization yield was not high. For example, with SE-8, only 83% dimer yield was achieved in 2000×10^{-3} M NaCl and 0.75×10^{-9} M origami concentrations (Figure 2a,e), whereas at 15×10^{-12} M SE-8 dimers start dissociating only below 40×10^{-3} M NaCl concentration (Figure 3a). Second, the length of the sticky ends clearly influenced the stability of the dimers in monomer-favorable conditions (Figure 3) but had no influence on the final dimerization yield in dimer-favorable conditions (250×10^{-3} M NaCl, Figure 2b). Therefore, we conclude that the incompletion of the dimerization reaction in dimer-favorable conditions is not a result of thermodynamic instability or of dissociation. Our dimer systems are rich with bridging strands, and as discussed below, this conclusion does not necessarily holds for dimers with fewer bridging strands.[30]

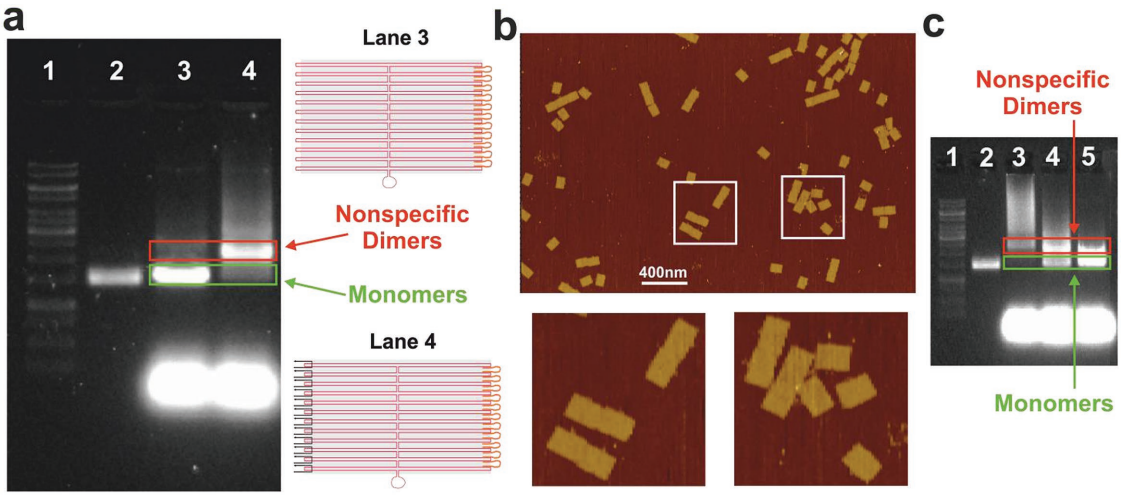

Figure 4. Nonspecific self-dimerization of origami monomers. a) Agarose gel chromatogram of 1-kb ladder, M13mp18 scaffold, origami-B without bridging strands, and origami-B with 23 bridging strands (SE-8) in lanes 1–4, respectively. b) AFM images of origami-B with 23 bridging strands. Origami-B with 23 bridging strands clearly forms nonspecific dimers. Some of the dimers are perfectly or almost perfectly aligned as shown in high magnification images. For more AFM images of nonspecific dimers, see Figure S7 of the Supporting Information. c) Agarose gel chromatogram of 1-kb ladder and M13mp18 scaffold in lanes 1 and 2, respectively, and origami-B SE-5, SE-8, and SE-11 (with 23 bridging strands) in lanes 3, 4, and 5, respectively.

2.8. Origami Monomer Structural Imperfections Are not a Major Reason for Low Dimerization Yield

Our data showed that dimer thermodynamic instability was not the reason for low dimerization yield, so we next evaluated whether monomer and dimer structural imperfections cause the low yield of our dimer systems. AFM images showed that about 7% of the monomers are visibly structurally defective with segments of the origami visibly missing (Figure S6, Supporting Information), an observation that is typical for origami constructs.[1] Furthermore, beyond the resolution of our AFM images, the origami constructs may be missing bridging strands[53] and bridging strands may be truncated.[54] Such structural imperfections potentially reduce dimer stability, and our dimer dissociation kinetic profiles provide evidence for these destabilizing mechanisms. The profiles show that at intermediate NaCl concentrations (for SE-8, for example, Figure 3a), dimer fractions plateau at values that are dependent on NaCl concentrations. This means that for a given intermediate NaCl concentration, some of the dimers dissociate and others do not (dimerization was not observed in these conditions, Figure S4 of the Supporting Information, and therefore, cannot explain the plateau). Thus, our data indicate that some of the dimers are less stable than the others. However, we will now explain why imperfections cannot explain the dimer low yields.

Our SE-5 dimer system has far fewer hybridizing nucleotides in comparison to the SE-11 (55% fewer base pairs), and yet achieved exactly the same dimerization yield in identical dimer-favorable conditions (80% yield, 250×10^{-3} M NaCl, Figure 2b). From these results, we conclude that only the absence of significant portion of the bridging strands would prevent dimerization in dimer-favorable conditions for our bridging strands-rich systems. Considering the low fraction of defective monomers observed in the AFM images (only 2–3% of the origami constructs are missing more than 50% of the interacting edges, and some of this damage may be due to the AFM tip, Figure S6 of the Supporting Information) and relative low probabilities of missing or significantly truncated bridging strands,[53,54] it is very unlikely that structural imperfections are responsible for more than a small fraction of the 14–20% unreactive monomers in our systems. Zenk et al. reported that polyacrylamide gel purification of the sticky end strands improves the dimerization yield by several percent;[30] however, this was for significantly fewer base pairs formed (4 strands of 6 nts length) than in our system. In fact, their rectangular origami system achieved ≈73% and 83% dimerization yields without and with purification, respectively. This comparison with our 23 × 11 base pairs system (SE-11), which achieved 80% dimerization yield, further supports the conclusion that thermodynamic instability and structural imperfections are unlikely to be major reasons for the low dimerization yields in our systems.

2.9. Monomer Nonspecific Self-Dimerization May Inhibit Correct Dimerization

As we established that thermodynamics instability and structural imperfections are unlikely to be major reasons for the low dimerization yields in our systems, we will now suggest an alternative mechanism. Agarose gel electrophoresis chromatograms and AFM images of origami-B monomers (SE-8) with 23 sticky end strands at one edge of the origami (and poly-T loops at the other edge) revealed the formation of many nonspecific homodimers (**Figure 4**a, lane 4 and Figure 4b and Figure S7 of the Supporting Information, respectively). In comparison, an agarose gel electrophoresis chromatogram of the same origami system without the bridging strands but with scaffold loops at one edge (and poly-T at the other edge) showed predominantly monomers (Figure 4a, lane 3). To understand the reason for

the origami self-dimerization, we measured self-dimerization for monomers with different lengths of sticky ends (SE-5, SE-8, and SE-11) using agarose gel electrophoresis. Interestingly, shorter sticky ends resulted in increased dimerization (Figure 4c, lanes 3, 4, and 5, respectively). We therefore suggest that the nonspecific interactions between origami monomers are not a result of nonspecific sticky end hybridization but rather result from blunt-end interactions. The edge of origami without sticky ends (and without edge staples) consists of scaffold loops (see schematic of the origami in Figure 4) that block blunt-end interactions. Nonlooped overhanging sticky ends strands can reside above and below the origami plain allowing stable blunt-end interactions. According to this model, shorter sticky ends would provide less hindrance to nonspecific interactions than longer sticky ends, in agreement with our results (Figure 4c).

In light of these results, we suggest that the low origami-A/origami-B dimerization yield is a result of the preformation of stable nonspecific homodimers. Although less stable than the correct dimers, these homodimers are stable enough to avoid dissociation and rearrangement to form correct dimers under our standard conditions. Recently, Tikhomirov et al. constructed an 8×8 origami array made of 64 unique origami tiles with dimerization yield of 95% using a small number of blunt-end interactions. To explain the high dimerization yield, the authors suggested that the weak blunt-end interactions allowed rearrangements that helped building blocks escape kinetic traps during array assembly.[40] Our AFM images show that for many of the nonspecific homodimers, the edges of the two monomers were perfectly or almost perfectly aligned, forming as many as 23 blunt-end interactions. Such blunt end-rich systems may not be able to rearrange to form correct dimers.

2.10. Achieving High Dimerization Yield

The addressability of origami building block attachment by blunt-end interactions is limited by the number of orthogonal origami shapes possible.[40] By contrast, strand hybridization that is based on specific Watson–Crick interactions is presumably significantly more orthogonal and should allow a higher degree of addressability as well as stronger attachment. The question, therefore, is how high dimerization yield can be achieved using strand hybridization? Gel electrophoresis purification of each monomer before mixing with the other would certainly remove nonspecific dimers. However, the success of such an approach may depend on whether nonspecific self-dimerization is an intrinsic reaction that will reoccur after purification or whether it is a result of the monomer preparation process (annealing). Treatment of the monomer at ion concentrations below that necessary for dimerization, increasing the ion concentration only after mixing of the two monomers, tuning the number and length of the bridging strands, and designing the origami edges to avoid nonspecific blunt-end interactions may prevent nonspecific monomer self-dimerization before mixing. We are currently investigating these options, and the initial results are very promising.

2.11. Summary of Origami Dimerization, Dimer Dissociation and Stability, and Dependence on Ions

Our study enabled us to identify the conditions in which dimers are formed and dissociate. For the SE-8 origami constructs, the dimerization threshold is 50×10^{-3} M NaCl (at 0.75×10^{-9} M monomer concentration, Figure 2a). At NaCl concentrations higher than 50×10^{-3} M, the reaction rate increased, but there were only minor increases in final yields (Figure 2e). Dimerization in the presence of 10×10^{-3} M Mg^{2+} resulted in 78% dimer yield with rates similar to that of dimerization in $70–80 \times 10^{-3}$ M NaCl ($k_{dim} = 1.87 \times 10^{6}$ M^{-1} s^{-1}). The origami dimerization rate was similar to the rate of dsDNA formation under identical conditions (250×10^{-3} M NaCl, Figure 2e). Dimer dissociation begins to occur at NaCl concentrations below about 40×10^{-3} M for the SE-8 origami (23×8 base pairs, Figure 3a) and at about 250×10^{-3} M for SE-5 (23×5 base pairs, Figure S5, Supporting Information). These findings are directly relevant to applications of DNA origami in biology as the ionic strength of a physiologically relevant solution is around that of solution containing $150–200 \times 10^{-3}$ M NaCl. Thus, a 23×5 dimer origami may dissociate in physiological conditions, whereas 23×8 dimers should be sufficiently stable. The dimerization rates of the SE-8 and WW-8 origami monomers were almost identical (Figure 2f), but the dimerization yield of the weaving welding was about 6% higher (Figure 2b). Under monomer-favorable conditions (15×10^{-3} M NaCl), the dissociation rate of the WW-8 dimers was up to tenfold slower than those of the SE-8 dimers (Figure 3b,c). Thus, the weaving welding technique formed somewhat more stable dimers than the sticky end technique when bridging strands were the same lengths. We note that designing sticky ends with different sequences and lengths is straightforward, whereas the weaving welding technique requires changes in the design of the origami itself, which is more costly and time consuming. This makes sticky ends a more suitable approach for Lego-like hierarchical origami building block assembly.

3. Conclusions

In this work, we established that the limited yield observed for dimerization of DNA origami monomers with a sufficient number of hybridization strands is not a result of dimer thermodynamic instability. Monomer structural imperfections are also unlikely account for more than a small percentage of the unreactive monomers and the low dimerization yields. We provide strong evidence for monomer self-dimerization, likely via blunt-end interactions made possible by the presence of bridging strands, and suggest that self-dimerization is the major reason for the limited yields of correct dimers. This model is in line with kinetic trap model previously suggested to explain high dimerization yields achieved using weak blunt-ends interactions. In light of our analysis, we propose investigating monomer purification and reduction of nonspecific dimerization by control of the number of bridging strands and the design of the origami edges and ion concentration as means to overcome the nonspecific dimerization interfering mechanism.

4. Experimental Section

Single-Molecule Fluorescence Experiment: Measurements of dimerization yields and of the dissociation kinetics were done on a KOH-treated coverslip that was sonicated (15 min) in 1 M KOH solution, thoroughly washed with distilled water, and dried with air. To prevent solution evaporation, the coverslip was sealed with silicone isolator sheet (Grace Bio-Labs), and, after sample deposition (≈40 µL), an upper coverslip was gently placed on the silicone sheet. The measurement buffer was comprised of 10×10^{-3} M Tris (pH 8), 1×10^{-3} M diaminoethane-tetraacetic acid (EDTA), 10 µg mL^{-1} bovine serum albumin (BSA) (Sigma-Aldrich; to reduce sample sticking), 1×10^{-3} M Trolox (Sigma-Aldrich; to reduce fluorophore photobleaching and photoblinking), and a desired NaCl concentration. Origami monomer (or dimer) concentration was 15×10^{-12} M.

Fitting the Kinetic Profiles—Dimerization Reactions: For fitting the dimerization profile data, a two-reactant second-order reaction model was assumed where origami-A and origami-B were present at equal concentrations

$$\mathrm{DATA}\left(\frac{S_{\mathrm{Dimer}}}{S_{\mathrm{Dimer}}+S_{\mathrm{Origami\text{-}B}}}\right)_t = \left(\left(1-\frac{1}{1+[A]_0\cdot k_{\mathrm{dim}}\cdot t}\right)\cdot DF_{\mathrm{inf}}\right) (1-BG_0)+BG_0 \quad (1)$$

where the two free parameters are the second order rate constant, k_{dim}, and the fraction of dimers in infinite time, DF_{inf}, also defined as reaction yield in this work. $[A]_0$ is monomer origami concentration at time zero, and BG_0 is background reading at time zero. The dimer fraction at time zero was attributed to background signal measured in a control experiment where origami-A and origami-B were mixed in the absence of bridging strands and was ≈12.5% for most experiments (see Figure S3, Supporting Information).

Fitting the Kinetic Profiles—Dissociation Reactions: For fitting the dimer dissociation profile data, a first-order reaction model was assumed

$$\mathrm{DATA}\left(\frac{S_{\mathrm{Dimer}}}{S_{\mathrm{Dimer}}+S_{\mathrm{Origami\text{-}B}}}\right)_t = \left(\left(1-DF_{\mathrm{inf}}\right)\cdot e^{-\frac{t}{\tau_{\mathrm{dis}}}}+DF_{\mathrm{inf}}\right) (DF_0-BG_0)+BG_0 \quad (2)$$

where the free parameters are the dissociation time constant, τ_{dis}, and the fraction of dimers in infinite time, DF_{inf}. The dimer fraction at time zero is DF_0 (typically, $DF_0 = \approx 0.8$).

Calculation of Experimental Error: Error bars in the dimer fraction measurements are the standard deviations calculated from three or more independent experiments measured under identical conditions. Error bars in k_{dim}, τ_{dis}, and DF_{inf} were determined by the fitting algorithm (Origin 8, OriginLab).

Agarose Gel Electrophoresis: Origami samples were loaded onto 1% agarose gel electrophoresis prepared from SeaKem LE agarose with 1 × tris-acetate-EDTA (TAE) buffer (pH 8.0) containing 12×10^{-3} M $MgCl_2$ and 0.01% (v/v) SybrSafe (Invitrogen) and subjected to a voltage of 70 mV for 2 h in an ice water bath.

AFM Imaging: For liquid-AFM imaging (Cypher, Asylum Research), 5–7 µL of the sample (12×10^{-3} M Mg^{2+} concentration) was deposited onto freshly cleaved mica and left to adsorb for 5 min. Then an additional 120–150 µL of TAE buffer containing 12×10^{-3} M $MgCl_2$ was added on top of the sample. Measurements were performed under ambient conditions on an active antivibration table in liquid tapping mode using HiRES-C14/AlBS, (MikroMasch) probe.

Supporting Information

Supporting Information is available from the Wiley Online Library or from the author.

Acknowledgements

This work was supported by grant from the Israel Science Foundation (1857/17). M.L. was supported by the Darom Fellowship and Y.B. was supported by the Negev Fellowship.

Conflict of Interest

The authors declare no conflict of interest.

Keywords

alternating laser excitation, DNA nanotechnology, DNA origami, origami tiling, single molecule fluorescence

Received: January 17, 2018
Revised: March 19, 2018
Published online:

[1] P. W. K. Rothemund, *Nature* **2006**, *440*, 297.
[2] M. R. Jones, N. C. Seeman, C. A. Mirkin, *Science* **2015**, *347*, 1260901.
[3] N. C. Seeman, H. F. Sleiman, *Nat. Rev. Mater.* **2018**, *3*, 17068.
[4] F. Hong, F. Zhang, Y. Liu, H. Yan, *Chem. Rev.* **2017**, *117*, 12584.
[5] B. Sacca, R. Meyer, M. Erkelenz, K. Kiko, A. Arndt, H. Schroeder, K. S. Rabe, C. M. Niemeyer, *Angew. Chem., Int. Ed.* **2010**, *49*, 9378.
[6] N. V. Voigt, T. Torring, A. Rotaru, M. F. Jacobsen, J. B. Ravnsbaek, R. Subramani, W. Mamdouh, J. Kjems, A. Mokhir, F. Besenbacher, K. V. Gothelf, *Nat. Nanotechnol.* **2010**, *5*, 200.
[7] K. Numajiri, M. Kimura, A. Kuzuya, M. Komiyama, *Chem. Commun.* **2010**, *46*, 5127.
[8] A. P. Eskelinen, A. Kuzyk, T. K. Kaltiaisenaho, M. Y. Timmermans, A. G. Nasibulin, E. I. Kauppinen, P. Torma, *Small* **2011**, *7*, 746.
[9] H. T. Maune, S. P. Han, R. D. Barish, M. Bockrath, W. A. Goddard, P. W. K. Rothemund, E. Winfree, *Nat. Nanotechnol.* **2010**, *5*, 61.
[10] M. Pilo-Pais, S. Goldberg, E. Samano, T. H. LaBean, G. Finkelstein, *Nano Lett.* **2011**, *11*, 3489.
[11] S. Pal, Z. T. Deng, H. N. Wang, S. L. Zou, Y. Liu, H. Yan, *J. Am. Chem. Soc.* **2011**, *133*, 17606.
[12] B. Q. Ding, Z. T. Deng, H. Yan, S. Cabrini, R. N. Zuckermann, J. Bokor, *J. Am. Chem. Soc.* **2010**, *132*, 3248.
[13] H. Bui, C. Onodera, C. Kidwell, Y. Tan, E. Graugnard, W. Kuang, J. Lee, W. B. Knowlton, B. Yurke, W. L. Hughes, *Nano Lett.* **2010**, *10*, 3367.
[14] S. Pal, Z. T. Deng, B. Q. Ding, H. Yan, Y. Liu, *Angew. Chem., Int. Ed.* **2010**, *49*, 2700.
[15] H. J. Liu, T. Torring, M. D. Dong, C. B. Rosen, F. Besenbacher, K. V. Gothelf, *J. Am. Chem. Soc.* **2010**, *132*, 18054.
[16] S. F. J. Wickham, M. Endo, Y. Katsuda, K. Hidaka, J. Bath, H. Sugiyama, A. J. Turberfield, *Nat. Nanotechnol.* **2011**, *6*, 166.
[17] S. F. J. Wickham, J. Bath, Y. Katsuda, M. Endo, K. Hidaka, H. Sugiyama, A. J. Turberfield, *Nat. Nanotechnol.* **2012**, *7*, 169.
[18] T. E. Tomov, R. Tsukanov, M. Liber, R. Masoud, N. Plavner, E. Nir, *J. Am. Chem. Soc.* **2013**, *135*, 11935.
[19] H. Z. Gu, J. Chao, S. J. Xiao, N. C. Seeman, *Nature* **2010**, *465*, 202.
[20] S. M. Douglas, I. Bachelet, G. M. Church, *Science* **2012**, *335*, 831.
[21] M. Endo, Y. Katsuda, K. Hidaka, H. Sugiyama, *Angew. Chem., Int. Ed.* **2010**, *49*, 9412.
[22] A. J. Thubagere, W. Li, R. F. Johnson, Z. Chen, S. Doroudi, Y. L. Lee, G. Izatt, S. Wittman, N. Srinivas, D. Woods, E. Winfree, L. Qian, *Science* **2017**, *357*, eaan6558.
[23] P. C. Nickels, B. Wunsch, P. Holzmeister, W. Bae, L. M. Kneer, D. Grohmann, P. Tinnefeld, T. Liedl, *Science* **2016**, *354*, 305.
[24] J. J. Funke, P. Ketterer, C. Lieleg, S. Schunter, P. Korber, H. Dietz, *Sci. Adv.* **2016**, *2*, e1600974.
[25] W. Liu, H. Zhong, R. Wang, N. C. Seeman, *Angew. Chem., Int. Ed.* **2011**, *50*, 264.

[26] R. Jungmann, M. Scheible, A. Kuzyk, G. Pardatscher, C. E. Castro, F. C. Simmel, *Nanotechnology* **2011**, *22*, 275301.
[27] Z. Li, L. Wang, H. Yan, Y. Liu, *Langmuir* **2012**, *28*, 1959.
[28] Z. Li, M. Liu, L. Wang, J. Nangreave, H. Yan, Y. Liu, *J. Am. Chem. Soc.* **2010**, *132*, 13545.
[29] T. C. Wu, M. Rahman, M. L. Norton, *Acc. Chem. Res.* **2014**, *47*, 1750.
[30] J. Zenk, C. Tuntivate, R. Schulman, *J. Am. Chem. Soc.* **2016**, *138*, 3346.
[31] J. Fern, J. Lu, R. Schulman, *ACS Nano* **2016**, *10*, 1836.
[32] Z. Zhao, Y. Liu, H. Yan, *Nano Lett.* **2011**, *11*, 2997.
[33] Y. Fu, J. Chao, H. Liu, C. Fan, *Chin. Sci. Bull.* **2013**, *58*, 2646.
[34] A. Rajendran, M. Endo, Y. Katsuda, K. Hidaka, H. Sugiyama, *ACS Nano* **2011**, *5*, 665.
[35] M. Endo, T. Sugita, Y. Katsuda, K. Hidaka, H. Sugiyama, *Chem. - Eur. J.* **2010**, *16*, 5362.
[36] M. Endo, T. Sugita, A. Rajendran, Y. Katsuda, T. Emura, K. Hidaka, H. Sugiyama, *Chem. Commun.* **2011**, *47*, 3213.
[37] M. Liber, T. E. Tomov, R. Tsukanov, Y. Berger, E. Nir, *Small* **2015**, *11*, 568.
[38] G. Tikhomirov, P. Petersen, L. Qian, *Nat. Nanotechnol.* **2017**, *12*, 251.
[39] S. Woo, P. W. K. Rothemund, *Nat. Chem.* **2011**, *3*, 620.
[40] G. Tikhomirov, P. Petersen, L. Qian, *Nature* **2017**, *552*, 67.
[41] T. Gerling, K. F. Wagenbauer, A. M. Neuner, H. Dietz, *Science* **2015**, *347*, 1446.
[42] N. Wu, I. Willner, *Nanoscale* **2017**, *9*, 1416.
[43] R. S. Wang, K. Gorday, C. Nuckolls, S. J. Wind, *Chem. Commun.* **2016**, *52*, 1610.
[44] T. E. Tomov, R. Tsukanov, Y. Glick, Y. Berger, M. Liber, D. Avrahami, D. Gerber, E. Nir, *ACS Nano* **2017**, *11*, 4002.
[45] X. Wei, J. Nangreave, Y. Liu, *Acc. Chem. Res.* **2014**, *47*, 1861.
[46] X. C. Bai, T. G. Martin, S. H. W. Scheres, H. Dietz, *Proc. Natl. Acad. Sci. USA* **2012**, *109*, 20012.
[47] R. M. Dirks, J. S. Bois, J. M. Schaeffer, E. Winfree, N. A. Pierce, *SIAM Rev.* **2007**, *49*, 65.
[48] T. E. Tomov, R. Tsukanov, R. Masoud, M. Liber, N. Plavner, E. Nir, *Biophys. J.* **2012**, *102*, 1163.
[49] R. Tsukanov, T. E. Tomov, M. Liber, Y. Berger, E. Nir, *Acc. Chem. Res.* **2014**, *47*, 1789.
[50] M. Zuker, *Nucleic Acids Res.* **2003**, *31*, 3406.
[51] L. E. Morrison, L. M. Stols, *Biochemistry* **1993**, *32*, 3095.
[52] Y. Gao, L. K. Wolf, R. M. Georgiadis, *Nucleic Acids Res.* **2006**, *34*, 3370.
[53] K. F. Wagenbauer, C. H. Wachauf, H. Dietz, *Nat. Commun.* **2014**, *5*, 3691.
[54] Integrated DNA Technologies, Chemical Synthesis and Purification of Oligonucleotides, https://www.Idtdna.Com/Pages/Docs/Technical-Reports/Chemical-Synthesis-of-Oligonucleotides.Pdf (accessed: June 2005).